AIAA JOURNAL
Vol. 40, No. 11, November 2002

Limit-Cycle Oscillation Induced by Nonlinear Aerodynamic Forces

K. W. Dotson,* R. L. Baker,† and B. H. Sako‡
The Aerospace Corporation, Los Angeles, California 90009-2957

The aerodynamic flow state on launch vehicle payload fairings and aircraft wings can change abruptly during transonic flight if the angle of attack reaches a critical value. The nonlinear pressure variation associated with a flow-state change induces transient structural responses that may converge to a limit-cycle oscillation (LCO). In this steady state, the work conducted during the flow-state changes balances the energy dissipation from structural damping. Analysis of this transonic LCO phenomenon is often conducted using a semi-empirical, unsteady pressure variation in which the levels for the flow states are determined from steady wind-tunnel test data. The presented theory addresses the condition in which the flow-state changes occur near a quasi-steady, nonzero angle of attack. The analysis for the resulting asymmetric forcing function complements the authors' existing derivations for a symmetric forcing function at zero angle of attack. Both the asymmetric and the symmetric analyses develop closed-form equations for the structural response frequency and amplitude. These expressions show that the solution space contains a subcritical Hopf bifurcation when the critical angle of attack equals the quasi-steady angle of attack. They also show that a saddle-node bifurcation, or fold, corresponds to the critical angle of attack beyond which LCO will not occur for a given quasi-steady angle of attack.

Nomenclature

AF	=	amplification factor, dimensionless
C_1–C_{10}	=	constants in complementary solution, dimensionless
$F(q)$	=	oscillating flow separation force, N
f	=	structural natural frequency, Hz
M	=	Mach number, dimensionless
n	=	aerodynamic stiffness, dimensionless
$\dot{n}$	=	aerodynamic damping, dimensionless
$q(t)$	=	generalized translation, m
t	=	time (transient motion), s
z	=	generalized translation normalized with respect to its static value, dimensionless
α	=	angle of attack, rad
Δt	=	time required for flow-state change, s
ζ	=	structural damping (as a ratio to the critical value), dimensionless
λ	=	eigenvalue of Jacobian matrix, 1/s
ξ	=	force variation, dimensionless
τ	=	time (steady-state motion), s
ϕ	=	structural mode value at location of flow-state change, rad/m
ω	=	undamped circular natural frequency, $2\pi f$, rad/s

Subscripts

a	=	asymmetric
a–d	=	time points in idealized force
cr	=	critical
e	=	excitation
l	=	linear, also force lag
m	=	mean
max	=	maximum
min	=	minimum
p	=	force pulse
s	=	symmetric
st	=	static
0	=	quasi steady

Received 21 June 2001; revision received 13 May 2002; accepted for publication 15 May 2002. Copyright © 2002 by the authors. Published by the American Institute of Aeronautics and Astronautics, Inc., with permission. Copies of this paper may be made for personal or internal use, on condition that the copier pay the $10.00 per-copy fee to the Copyright Clearance Center, Inc., 222 Rosewood Drive, Danvers, MA 01923; include the code 0001-1452/02 $10.00 in correspondence with the CCC.

*Senior Engineering Specialist, Structural Dynamics Department, P.O. Box 92957–M4/911. Associate Fellow AIAA.

†Senior Engineering Specialist, Fluid Mechanics Department, P.O. Box 92957–M4/967.

‡Senior Engineering Specialist. Structural Dynamics Department, P.O. Box 92957–M4/911.

Introduction

WIND-TUNNEL tests show that the flow at the cone–cylinder junction of launch vehicle payload fairings can oscillate between separated and attached states.[1,2] Flow-state changes also occur on aircraft wings due to shock-induced trailing-edge separation.[3–5] Oscillations between the attached and separated flow states occur within fixed ranges of angle of attack and transonic Mach number.[2,4]

For both launch vehicles and aircraft, the transition from one flow state to another occurs fairly rapidly with respect to the structural response, such that the corresponding aerodynamic force change is steplike.[3,6] The flow-state transitions, moreover, are triggered when the local angle of attack reaches a critical value.[2,4] Because of the time required for development of the flow state, the nonlinear aerodynamic force lags the structural response.[3,6] The phenomenon is, therefore, characterized by steplike forces that trail the critical response value by a small time Δt. This time lag introduces energy to the system,[3,6] and given sufficient time for convergence, the fluid–structure interaction can lead to limit-cycle oscillation (LCO). In this steady state, the work conducted during the force lags balances the energy dissipation from structural damping.[6]

Semi-empirical models of the fluid–structure interaction have been used for analysis of launch vehicle[6–9] and aircraft[3–5] LCO. In this approach, steady experimental or analytical data are used to quantify the attached and separated flow pressure distributions. The unsteady force variation is based on a critical rotation angle for flow-state changes and a finite rise time. For example, the model shown in Fig. 1 has been used for zero-angle-of-attack flight.[6–9] In this case, the flow-state changes occur symmetrically, that is, they are identical on both sides of the structure at the critical angle of attack. The forcing function ξ is supported by flight pressure measurements, from which the time lag value can be estimated.[7]

Analytic expressions for response amplitude and frequency are developed in Refs. 6–9 for symmetrically driven LCO, with an emphasis on launch vehicle applications. Similar expressions are developed herein for asymmetrically driven LCO using the model shown in Fig. 2. That is, the presented theory is intended for analysis of flow-state oscillations that occur on one side of a structure subjected

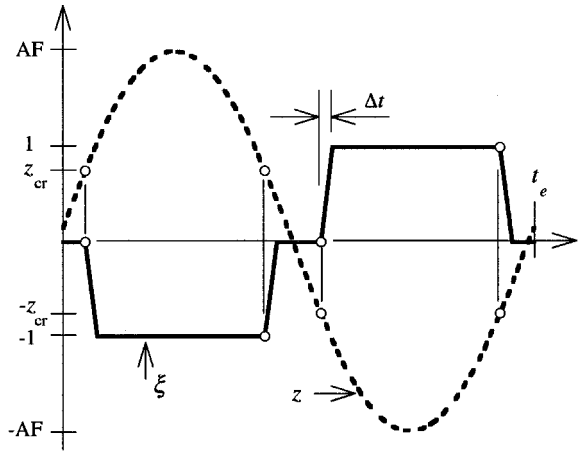

Fig. 1 One cycle of coupled force and response in semiempirical analysis at 0-deg angle of attack.

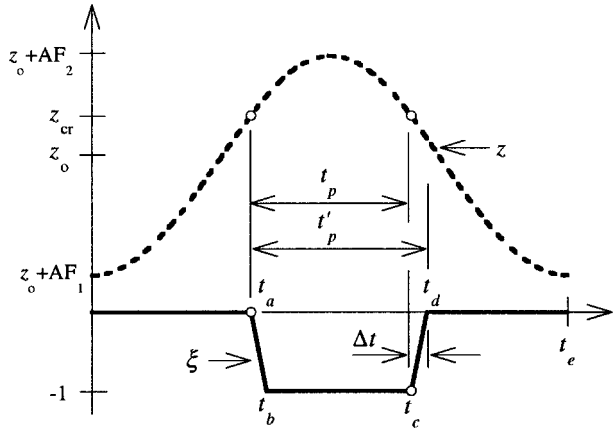

Fig. 2 One cycle of coupled force and response in semiempirical analysis at nonzero angle of attack.

to a quasi-steady angle of attack. The semi-empirical analysis of aircraft LCO also employs an asymmetric, steplike forcing function that lags the structural response, but only numerical solutions of the equation of motion are presented in Refs. 3–5. The formulation herein is general. It is believed that the presented closed-form expressions and parametric studies are applicable to any dynamic phenomenon that can be approximated by Fig. 2.

The semi-empirical methods for aircraft LCO have been validated using flight-test data.[3–5] Trends in these results generally support the relationships presented herein, and it appears that extant aircraft test data and semi-empirical predictions could be used to confirm the present theory. Wind-tunnel testing directed toward validation of models for launch vehicle LCO has been initiated,[10] but currently there is a paucity of associable flight pressure and acceleration measurements.[7]

Equation of Motion

Launch vehicle LCO[7] is commonly predominated by aeroelastic coupling with a single system mode. Although aircraft LCO occurs for a single mode in many cases, it can involve at least two modes with a flutterlike coupling. The single structural mode corresponds to core bending for launch vehicle LCO[7] and to wing bending or torsion for aircraft LCO.[3] For multiple-mode aircraft LCO, the coupling involves some combination of bending and torsion. Recent computational results for wings in inviscid flow, nevertheless, show that a single-degree-of-freedom torsion flutter instability, rather than classical bending–torsion coalescence flutter, characterizes the bottom of the transonic dip.[11] Provided that a single mode does indeed predominate, the equation of motion for the coupled system is defined by

$$\ddot{q}(t) + 2\zeta\omega\dot{q}(t) + \omega^2 q(t) = F(q) \tag{1}$$

The generalized force $F(q)$ is a function of the structural response because the flow state changes at a critical response value. The amplitude F of the generalized force is defined by profiles of the pressure coefficient for the separated and attached flow states. Dotson et al.[6] discuss, at length, the use of steady wind-tunnel data or steady computational fluid dynamics (CFD) results for the calculation of this amplitude. Normalizing Eq. (1) with respect to the static value $q_{st} = F/\omega^2$ yields

$$\ddot{z}(t) + 2\zeta\omega\dot{z}(t) + \omega^2 z(t) = \omega^2\xi(z) \tag{2}$$

where the nondimensional force variation ξ is herein defined by the model shown in Fig. 2.

Initial and Critical Values

The quasi-steady angle of attack is converted into the following nondimensional modal displacement:

$$z_0 = \alpha_0/\phi q_{st} \tag{3}$$

This deflection is added to the dynamic response from Eq. (2), such that the total response corresponding to the critical rotation is given by

$$z_{cr} = \alpha_{cr}/\phi q_{st} \tag{4}$$

The scenario shown in Fig. 2, in which z_0 and z_{cr} are positive values and $z_{cr} > z_0$, is used throughout this work. It is easy to show that negative values of z_0 and z_{cr} (and/or scenarios with $z_{cr} < z_0$) can also be evaluated using the analytical expressions presented herein. Note that the model implies that the quasi-steady angle of attack is large enough that the minimum response never exceeds $-z_{cr}$. If this were to occur, positive and negative force pulses (of generally different width) would exist.

Numerical Algorithm

Equation (2) is solved numerically herein to provide comparisons with the presented closed-form analytical expressions. The algorithm applies the procedures outlined in Ref. 12 for numerical analysis of oscillators with motion-dependent discontinuities.

The computer code establishes the initial segment of the function ξ based on the initial response value, that is, the value of $z(0)$ determines whether $\xi(0) = 0$ or -1. The initial velocity, which can be arbitrary, does not affect the force variation because the flow-state changes are defined only by a critical displacement value.

Given the initial segment of the force variation, the response is computed and checked at each time step to establish the point at which the response reaches z_{cr}. The appropriate segment of the ξ function is then added to the initial segment, and the time march continues until the response again reaches z_{cr}. The resulting response and force variation, thus, satisfy the fluid–structure interaction implicit in Fig. 2.

Although application of this algorithm is slower than that used in Refs. 6 and 8, it eliminates deficiencies that can occur when the initial conditions are close to the unstable limit-cycle state.[6] The values z_0 and z_{cr} in the examples herein are arbitrarily chosen but are credible, depending on the parameters in Eqs. (3) and (4).

Phase-Plane Characteristics

Figure 3 shows phase-plane diagrams constructed using the numerical algorithm. The trajectories (light solid lines) are shown in three separate parts to facilitate comparisons with Fig. 4.

The quasistatic displacement z_0 is generally a stable fixed point. The heavy solid and dashed lines in Fig. 3a represent stable and unstable limit cycle states, respectively. It is shown in a latter section that, as the control parameter z_{cr}–z_0 increases, the unstable limit cycle expands and the stable limit cycle contracts until they meet at a fold, or saddle-node bifurcation of cycles.

Time histories corresponding to the trajectories in Fig. 3 are plotted in Fig. 4. Figure 4a shows how all initial conditions that lie within the unstable limit cycle yield force pulses that decrease in width, until the response amplitude falls below z_{cr}. After this time, the function ξ disappears, and the response approaches the stable

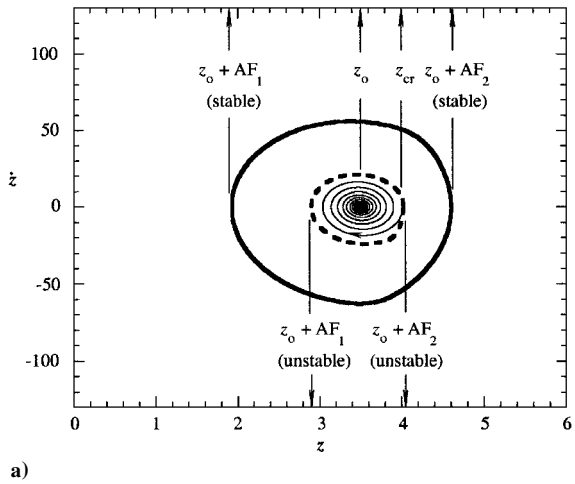

a)

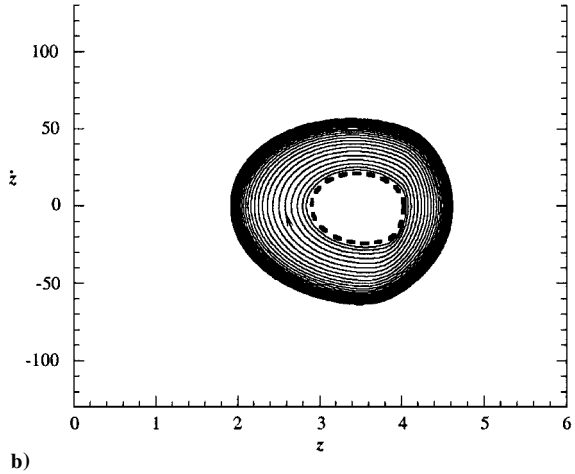

b)

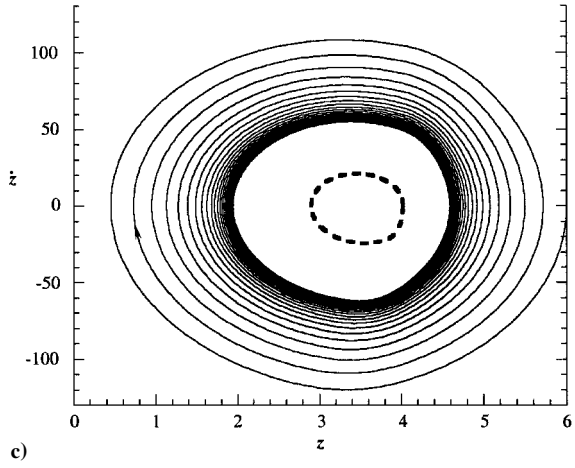

c)

Fig. 3 Phase plane diagrams constructed from subset of displacement histories shown in Fig. 4: a) initial conditions inside of unstable limit cycle, b) initial conditions outside of unstable limit cycle, and c) initial conditions outside of stable limit cycle.

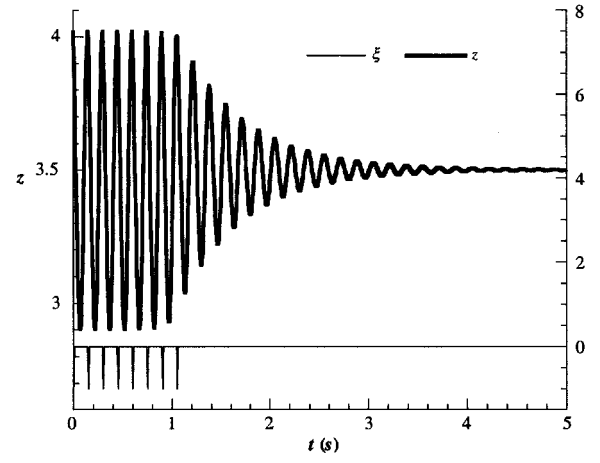

a) $z(0) = 4.018$

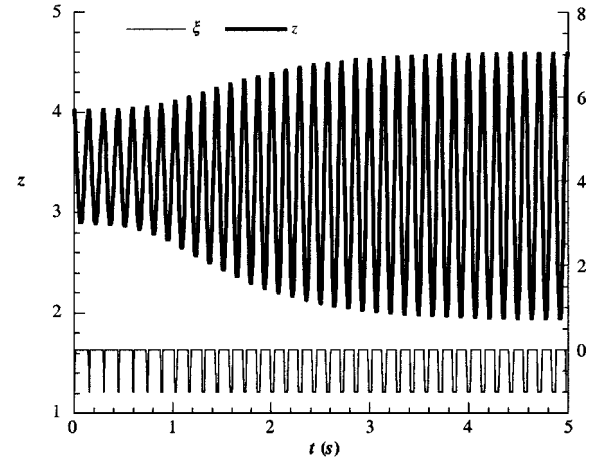

b) $z(0) = 4.019$

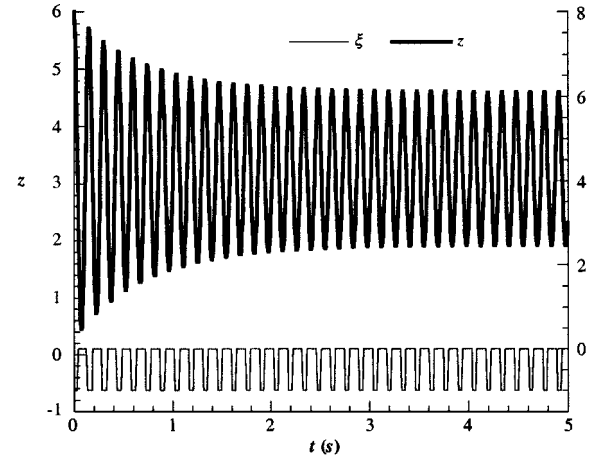

c) $z(0) = 6$

Fig. 4 Displacement and force histories from numerical algorithm where f = 6 Hz, ζ = 4%, Δt = 10 ms, z_{cr} = 4, z_0 = 3.5, and $\dot{z}(0) = 0$.

fixed point z_0 through free vibration. Figure 4b shows how all initial conditions that lie outside of the unstable limit cycle, but within the stable limit cycle, yield force pulses that increase in width and a response that approaches the stable limit cycle. Finally, Fig. 4c shows how all initial conditions that lie outside of the stable limit cycle yield force pulses that decrease in width and a response that approaches the stable limit cycle.

Limit-Cycle Response

It is evident from Figs. 1 and 2 that the self-excitation of a structural mode due to nonlinear aerodynamic forces can be modeled as a dynamic system with motion-dependent discontinuities. Many mechanical problems fall under this rubric, including systems with working clearances, oscillators with coulomb friction, and impact-type structural elements.[12]

More specifically, Eq. (2) describes a single-degree-of-freedom oscillator excited by a piecewise linear force. Discontinuities in stiffness and damping are more common in mechanical systems than external motion-dependent forces,[13] but the equations of motion for such "piecewise linear oscillators" are formulated in the same way as Eq. (2).[14] As shown in Ref. 8, and briefly discussed in a later section

of this paper, nonlinear aerodynamic forces can also be converted if desired into equivalent, discontinuous aerodynamic stiffness and damping terms.

Natsiavas[14] claims that motion-dependent forces must be expanded using a Fourier series. If force discontinuities exist, an infinite number of terms comprise the Fourier series. The contributions of the terms in the expansion are then added to establish the particular solution in each time interval. In practice, a finite number of Fourier terms are retained, which introduces error into the system response and any derived results.

The approach advocated in Ref. 14 is classical, but is not used hereinafter. Instead, a direct, closed-form solution of Eq. (2) is established for the steady states. The analytical expressions are then used to study parametrically single-degree-of-freedom LCO induced by nonlinear aerodynamic forces, that is, by forces that are steplike, that are asymmetric, and that lag the response.

Multifrequency Trial Function

In Ref. 15 it is shown that the exact steady-state response of linear systems subjected to analytic forces can be derived in closed form by satisfying the governing differential equation and periodicity condition. This approach is used herein to establish a multifrequency trial function based on the piecewise-linear force ξ shown in Fig. 2. The resulting linear solution is then made to satisfy the force–response coupling and, hence, the nonlinear equation of motion. The response period is an adjustable parameter, defined as the value that balances the work conducted during the force lags and the energy dissipation from structural damping.

The low damping values typical of launch vehicle[6] and aircraft[3,4] structural modes do not significantly affect the linear steady-state response, provided the excitation and natural frequencies are not almost identical.[6,15] It will be shown that, although the effect of structural damping on the multifrequency trial function is negligible, it plays a critical role in establishing the excitation period.

Response History

The steady-state response for an undamped linear oscillator subjected to the forcing function in Fig. 2 is given by

$$z_l(\tau) = C_1 \sin(\omega\tau) + C_2 \cos(\omega\tau), \qquad 0 \le \tau \le t_a \tag{5a}$$

$$z_l(\tau) = C_3 \sin(\omega\tau) + C_4 \cos(\omega\tau) - (\tau - t_a)/\Delta t \qquad t_a \le \tau \le t_b \tag{5b}$$

$$z_l(\tau) = C_5 \sin(\omega\tau) + C_6 \cos(\omega\tau) - 1, \qquad t_b \le \tau \le t_c \tag{5c}$$

$$z_l(\tau) = C_7 \sin(\omega\tau) + C_8 \cos(\omega\tau) - 1 + (\tau - t_c)/\Delta t \qquad t_c \le \tau \le t_d \tag{5d}$$

$$z_l(\tau) = C_9 \sin(\omega\tau) + C_{10} \cos(\omega\tau), \qquad t_d \le \tau \le t_e \tag{5e}$$

where τ designates the steady-state timescale with an origin at the beginning of any given response cycle.

The 10 unknown constants in Eq. (5) must satisfy displacement and velocity continuity at the segment interfaces. They must also satisfy the periodicity conditions $z_l(0) = z_l(t_e)$ and $\dot{z}_l(0) = \dot{z}_l(t_e)$, that is, by definition, the responses at the beginning and end of the cycle are identical. It can be shown that the following constants satisfy these 10 constraints:

$$C_1 = 0 \tag{6a}$$

$$(\omega\Delta t)C_2 = \sin(\omega t_a) - \sin(\omega t_b) + \cot(\omega t_e/2)[\cos(\omega t_a) - \cos(\omega t_b)] \tag{6b}$$

$$(\omega\Delta t)C_3 = \cos(\omega t_a) \tag{6c}$$

$$(\omega\Delta t)C_4 = \cot(\omega t_e/2)[\cos(\omega t_a) - \cos(\omega t_b)] - \sin(\omega t_b) \tag{6d}$$

$$(\omega\Delta t)C_5 = \cos(\omega t_a) - \cos(\omega t_b) \tag{6e}$$

$$(\omega\Delta t)C_6 = \cot(\omega t_e/2)[\cos(\omega t_a) - \cos(\omega t_b)] \tag{6f}$$

$$(\omega\Delta t)C_7 = \cos(\omega t_a) - [1 + \cos(\omega t_e)]\cos(\omega t_b) - \sin(\omega t_e)\sin(\omega t_b) \tag{6g}$$

$$(\omega\Delta t)C_8 = \cot(\omega t_e/2)[\cos(\omega t_a) - \cos(\omega t_b)] + \sin(\omega t_e)\cos(\omega t_b) - \cos(\omega t_e)\sin(\omega t_b) \tag{6h}$$

$$(\omega\Delta t)C_9 = [1 + \cos(\omega t_e)][\cos(\omega t_a) - \cos(\omega t_b)] + \sin(\omega t_e)[\sin(\omega t_a) - \sin(\omega t_b)] \tag{6i}$$

$$(\omega\Delta t)C_{10} = \cos(\omega t_e)[\sin(\omega t_a) - \sin(\omega t_b)] + \cos(\omega t_e)\cot(\omega t_e/2)[\cos(\omega t_a) - \cos(\omega t_b)] \tag{6j}$$

The linear response defined by Eq. (5) is symmetric about the midpoint of the force ξ and, hence, does not satisfy the displacement constraints indicated by the circles in Fig. 2. The trial function, however, is admissible, if it is shifted in the direction of the origin by an amount equal to half of the time lag. The nonlinear response is, therefore, taken as

$$z = z_l(\tau + \Delta t/2) \tag{7}$$

The difference in the midpoints of the nonlinear response and the force ξ affects subsequent derivations of the force pulse width t_p.

For launch vehicle[7] and aircraft[3] LCO, the time lag Δt is generally small relative to the period of the structural mode ($T = 1/f = 2\pi/\omega$). In such cases, the simplification $\omega\Delta t \approx 0$ is justified, which implies that the force ξ can be approximated by a pure step function. Thus, $t_a \approx t_b$, $t_c \approx t_d$, and Eqs. (5b) and (5d) become irrelevant. It can be shown that the remaining constants in Eq. (6), in this case, reduce to

$$C_1 = 0 \tag{8a}$$

$$C_2 = \cot(\omega t_e/2)\sin(\omega t_a) - \cos(\omega t_a) \tag{8b}$$

$$C_5 = \sin(\omega t_a) \tag{8c}$$

$$C_6 = \cot(\omega t_e/2)\sin(\omega t_a) \tag{8d}$$

$$C_9 = [1 + \cos(\omega t_e)]\sin(\omega t_a) - \sin(\omega t_e)\cos(\omega t_a) \tag{8e}$$

$$C_{10} = \cos(\omega t_e)[\cot(\omega t_e/2)\sin(\omega t_a) - \cos(\omega t_a)] \tag{8f}$$

The linear response defined by Eq. (8) can also be used to generate a semi-empirical model in which a pure step force lags the critical response by the time Δt. Indeed, in its simplest form, the aircraft LCO methodology uses this model of the flow-state transitions.[3]

Response Amplitude

It can be shown that the minimum and maximum of the linear response are located at the origin and at the midpoint of the period, respectively. The following amplification factors (AFs) are expressions for these values derived using Eqs. (5a) and (5c):

$$\mathrm{AF}_1 = \left[\frac{1 - \cos(\omega\Delta t)}{\omega\Delta t}\right]\frac{\cos(\omega t_p'/2)}{\sin(\omega t_e/2)} - \left[\frac{\sin(\omega\Delta t)}{\omega\Delta t}\right]\frac{\sin(\omega t_p'/2)}{\sin(\omega t_e/2)} \tag{9a}$$

$$\mathrm{AF}_2 = -1 + \left[\frac{1 - \cos(\omega\Delta t)}{\omega\Delta t}\right]\frac{\cos[\omega(t_e - t_p')/2]}{\sin(\omega t_e/2)} + \left[\frac{\sin(\omega\Delta t)}{\omega\Delta t}\right]\frac{\sin[\omega(t_e - t_p')/2]}{\sin(\omega t_e/2)} \tag{9b}$$

where t_p' is the pulse width including the force ramps (Fig. 2), such that

$$t_p' = t_p + \Delta t, \qquad t_e = 2t_a + t_p' \tag{10}$$

The maximum and minimum responses are expressed as AFs because the equation of motion was normalized with respect to the

static displacement. When the simplification $\omega\Delta t \approx 0$ is introduced, Eq. (9) reduces to

$$\mathrm{AF}_1 = -\frac{\sin(\omega t_p/2)}{\sin(\omega t_e/2)} \tag{11a}$$

$$\mathrm{AF}_2 = -1 + \frac{\sin[\omega(t_e - t_p)/2]}{\sin(\omega t_e/2)} \tag{11b}$$

When added to z_0, Eq. (9) predicts the values on the z axis for the unstable and stable limit-cycle states (see Fig. 3a). The parameters t_p and t_e, however, must be established before Eq. (9) can be evaluated.

Force Pulse Width

As shown in Fig. 2, the time point at which the response reaches the critical deflection defines the duration of the dead zone in the force ξ and, by association, the pulse width t'_p. The response at t_a, therefore, must satisfy the constraint

$$z_{\mathrm{cr}} = z_l(t_a + \Delta t/2) + z_0 = C_2 \cos[\omega(t_a + \Delta t/2)] + z_0 \tag{12}$$

Evaluating Eq. (12) yields

$$z_{\mathrm{cr}} - z_0 = \left\{\left[\frac{1 - \cos(\omega\Delta t)}{\omega\Delta t}\right]\cos\left(\frac{\omega t'_p}{2}\right) - \left[\frac{\sin(\omega\Delta t)}{\omega\Delta t}\right]\sin\left(\frac{\omega t'_p}{2}\right)\right\}\frac{\cos[\omega(t_e - t'_p + \Delta t)/2]}{\sin(\omega t_e/2)} \tag{13}$$

The solution t'_p/t_e can be determined from Eq. (13), when the values z_{cr}–z_0 and ωt_e are given. The simplification $\omega\Delta t \approx 0$ applied to Eq. (13) yields the following explicit expression for the pulse width:

$$t_p/t_e = \frac{1}{2} + \frac{(\pm\beta - \pi/2)}{\omega t_e} \tag{14}$$

where $t'_p \approx t_p$ and

$$\beta = \cos^{-1}[p \sin(\omega t_e/2)], \qquad 0 \le \beta \le \pi/2 \tag{15a}$$

$$p = 2(z_{\mathrm{cr}} - z_0) + 1 \tag{15b}$$

There are two admissible t'_p values. The smaller value corresponds to the unstable limit cycle, whereas the larger value corresponds to the stable limit cycle (see Fig. 4). This conclusion is intuitive because narrow force pulses produce smaller response amplitudes than do wide pulses for a linear oscillator.[6]

Response Period

The final parameter required for the multifrequency solution is the excitation period t_e. At the limit-cycle state, energy dissipation from structural damping is exactly balanced by work conducted by the force ξ. This requirement leads to the identity

$$\int_{z(0)}^{z(t_e)} 2\zeta\omega\dot{z}\,\mathrm{d}z = \omega^2 \int_{z(0)}^{z(t_e)} \xi\,\mathrm{d}z \tag{16}$$

Figure 5 shows the variation of the force ξ with displacement z. The hysteretic loop, depicted by the shaded rhomboid, is a result of the flowfield time lag. According to Eq. (16), the net work conducted during a response cycle equals the scaled area within the hysteretic loop. It is readily apparent that the work conducted in the semi-empirical model is dependent on the assumed force–response relationship. For example, a pure step force that lags the critical response by an amount Δt produces a rectangular hysteretic loop with twice the area of the rhomboid in Fig. 5.

A clockwise hysteretic loop corresponds to an aerodynamic force that is out of phase with the response, as shown in Fig. 2. According to the directions of z and ξ, and the integral on the right-hand side of Eq. (16), force–response coupling of this type does positive net work during the time lag Δt. Conversely, an aerodynamic force that is in phase with the structural response generates a counterclockwise hysteretic loop and does negative net work. It has been recognized for both launch vehicle[8,9] and aircraft[4] LCO that opposition of the force and response, that is, the presence of a clockwise hysteretic loop, corresponds to negative aerodynamic damping.

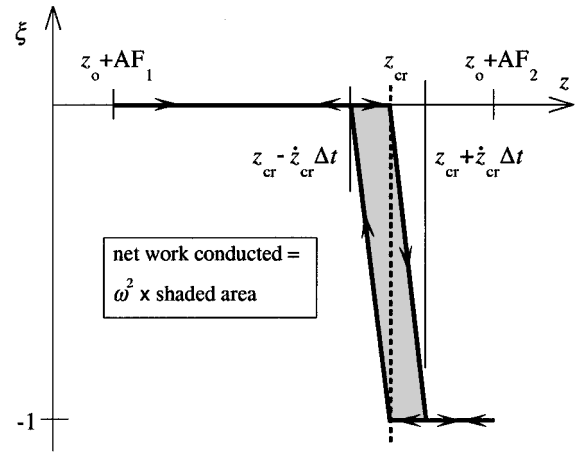

Fig. 5 Hysteresis due to flowfield time lag.

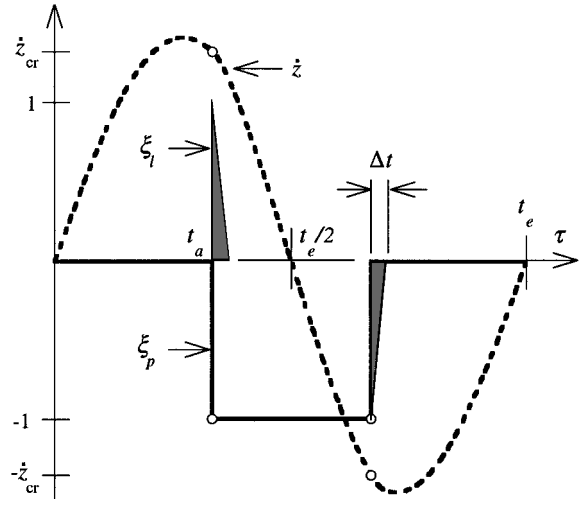

Fig. 6 Decomposition of semi-empirical force into pulse and lags.

Equation (16) can also be expressed in the time domain as

$$\int_0^{t_e} 2\zeta\omega\dot{z}^2\,\mathrm{d}\tau = \omega^2 \int_0^{t_e} \xi\dot{z}\,\mathrm{d}\tau \tag{17}$$

Figure 6 shows the decomposition of the exciting force into a pulse and lags, such that $\xi = \xi_l + \xi_p$. The pulse component represents the force variation for instantaneous flow-state changes at the critical response value, whereas the lag component represents the change to the force pulse affected by the aerodynamic time lag.[8,9]

Note that the two shaded parts of the function ξ_l would be rectangular (rather than triangular) if the force–response coupling were modeled by a pure step function that lags the critical response value. These rectangles would also have twice the area, reflecting that twice the net work is conducted in a pure step model.

Because the velocity shown in Fig. 6 is symmetric about the response-adjusted cycle midpoint, the net work conducted by the force pulse ξ_p equals zero. Equation (17), therefore, simplifies to

$$2\zeta\omega \int_0^{t_e} \dot{z}^2\,\mathrm{d}\tau = \omega^2 \int_0^{t_e} \xi_l\dot{z}\,\mathrm{d}\tau \approx \omega^2\dot{z}_{\mathrm{cr}}\Delta t \tag{18}$$

which dictates that the following relationship must be satisfied by the excitation period:

$$\int_0^{t_e} \left(\dot{z}^2/\dot{z}_{\mathrm{cr}}\right)\mathrm{d}\tau = \frac{\omega\Delta t}{2\zeta} \tag{19}$$

Note that the right-hand side of Eq. (19) would be twice as large for the aforementioned pure step force–response coupling model.

It can be shown that substitution of the simplified trial function [Eq. (8)] into Eq. (19) yields

$$-\left\{\frac{\omega(t_e-t_p)/2}{\sin[\omega(t_e-t_p)/2]}\right\}\left\{\frac{\sin[\omega(t_e/2-t_p)]}{\sin(\omega t_p/2)}\right\}$$
$$+\left[\frac{\omega t_e/2}{\sin(\omega t_e/2)}\right]\left\{\frac{\sin[\omega(t_e-t_p)/2]}{\sin(\omega t_p/2)}\right\}=1+\frac{\omega\Delta t}{2\zeta} \qquad (20)$$

The pulse width t_p can be eliminated from Eq. (20) through substitution of Eq. (14). The excitation period is, therefore, the value t_e that satisfies the relationship

$$\left[\frac{\omega t_e/2}{\sin(\omega t_e/2)}\right]\left[\frac{1+p}{\pm\sin\beta-p\cos(\omega t_e/2)}\right]$$
$$+\frac{p(\pm\beta-\omega t_e/2-\pi/2)\sin(\omega t_e/2)}{\pm\sin\beta-\cos(\omega t_e/2)}=1+\frac{\omega\Delta t}{2\zeta} \qquad (21)$$

where the positive and negative signs in the symbol $\pm$ are applied for the stable and unstable limit-cycle states, respectively. The excitation periods for these limit cycles, in other words, are not identical.

Accuracy of Solution

The multifrequency technique is exact for linear systems subjected to periodic, analytic forcing functions.[15] The results are, thus, identical to those based on Fourier analysis, if all of the harmonic terms in the series expansions are retained.[15] For piecewise-linear forces of the type shown in Fig. 2, this means that an infinite number of harmonic terms are required in Fourier analysis to achieve the accuracy of the closed-form expressions from the multifrequency technique.

Similarly, harmonic balance (HB) is often used to analyze nonlinear equations of motion,[16] but can be quite cumbersome as the number of harmonic terms increases. An HB solution is derived in the Appendix using only the leading term in the Fourier expansion of the force ξ. The objective of including the HB derivation is to assess the loss of accuracy inherent in first-order harmonic solutions for the semi-empirical LCO model, to inspire confidence in the less well-known multifrequency technique, and to develop useful relationships for the limits of the solution space.

Table 1 compares results from the closed-form expressions with numerical solutions of Eq. (2). A 3-Hz mode with 1% of critical structural damping and a 10-ms aerodynamic time lag is assumed. The values z_{cr} and z_0 are taken as 5 and 4, respectively. The simplification $\omega\Delta t \approx 0$ is used in neither the multifrequency nor the HB solution.

The comparison indicates that the multifrequency and numerical results are in very good agreement for both the stable and unstable limit-cycle states. The 1–2% error in the amplification factors for the multifrequency solution is attributed to the effects of structural damping on the shape of the trial function [Eq. (5)]. For this example, first-order HB is significantly less accurate than the multifrequency solution. The 7–30% error in the tabulated AFs is caused by truncation in the Fourier series expansion of the force variation ξ [Eq. (A1)].

Table 1 Analytical and numerical results for example problem (f = 3 Hz, ζ = 1%, Δt = 10 ms, z_{cr} = 5, and z_0 = 4)

		Analytical	
Parameter	Numerical	Multifrequency	HB
	Stable limit cycle		
ft_e	0.914	0.914	0.908
t'_p/t_e	0.370	0.372	0.359
AF_1	−3.07	−3.10	−2.88
AF_2	2.52	2.55	2.23
z_{max}	6.52	6.55	6.23
z_{min}	0.93	0.90	1.12
	Unstable limit cycle		
ft_e	0.940	0.944	0.908
t'_p/t_e	0.103	0.095	0.171
AF_1	−1.09	−1.07	−1.39
AF_2	1.04	1.03	1.12
z_{max}	5.04	5.03	5.12
z_{min}	2.91	2.93	2.61

Parametric Studies

The effects of the system parameters on the LCO are investigated in this section. For the sake of clarity, only the analytical expressions with the simplification $\omega\Delta t \approx 0$ are used. The effects of $\omega\Delta t$ are considered secondary and beyond the scope of this work but could be studied using the equations presented herein.

Figure 7 shows the nondimensional excitation period ft_e as a function of the key ratio $f\Delta t/\zeta$. Figures 7–10 can be used for other models of the force transition by applying a scale factor to the value $f\Delta t/\zeta$. The magnitude of the scale factor equals the area of the hysteretic loop in the force transition model divided by that for ramped force transitions. For example, the value $f\Delta t/\zeta$ would be scaled up by a factor of two for pure step force transitions because the corresponding hysteretic loop has twice the area of that shown in Fig. 5.

Note that a lower bound at $f\Delta t/\zeta \approx 2(z_{cr}-z_0)$ exists. Below this value, the work conducted during the force lags cannot balance the energy dissipation from structural damping. The excitation

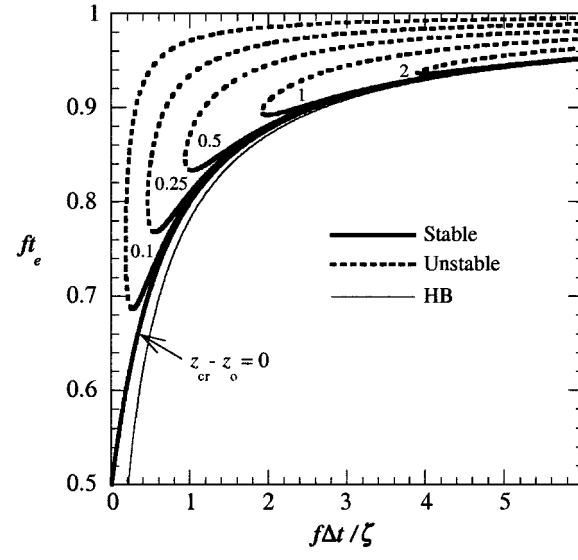

Fig. 7 Nondimensional excitation period for stable and unstable limit-cycle states.

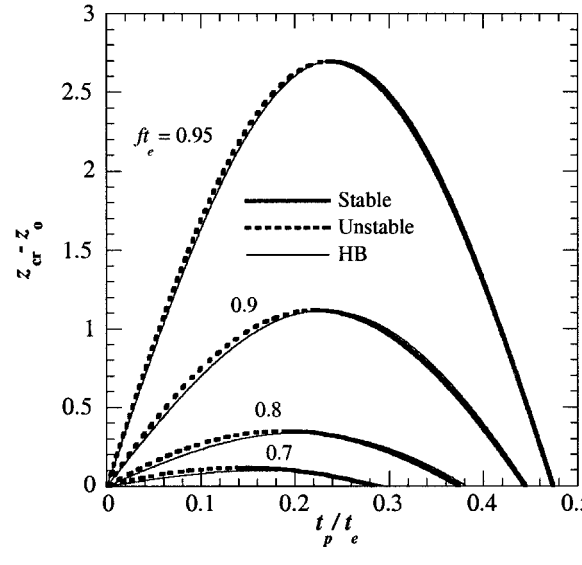

Fig. 8 Nondimensional force pulse width for stable and unstable limit-cycle states.

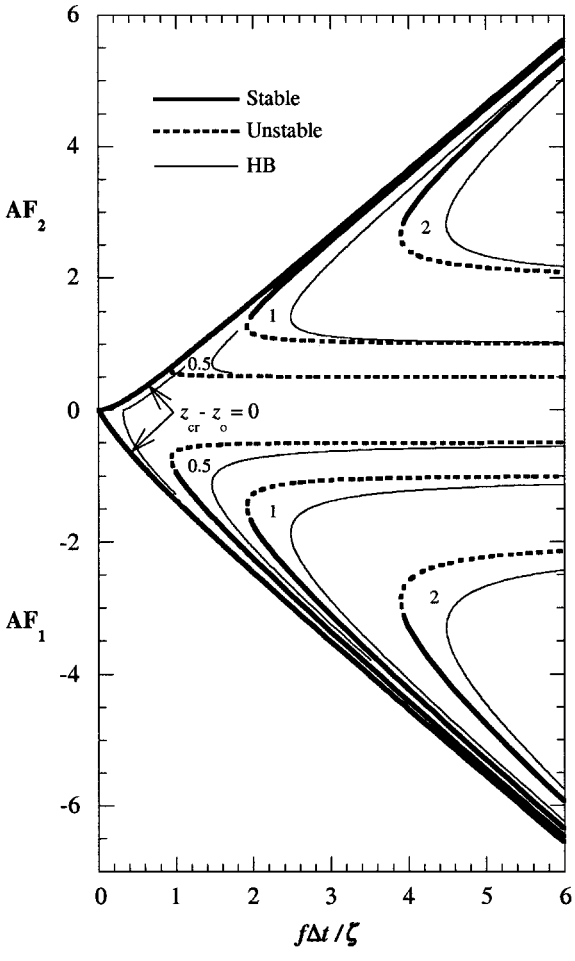

Fig. 9 AFs for stable and unstable limit-cycle states.

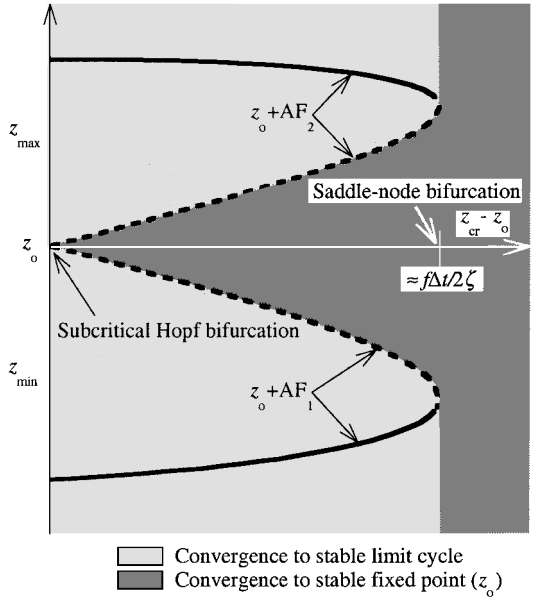

Fig. 10 Bifurcation diagram based on multifrequency solution.

frequency for unstable and stable limit cycles are not equal [see Eq. (21)], but the first-order HB solution fails to predict this difference [see Eq. (A6)]. As the ratio $f\Delta t/\zeta$ increases, all of the curves in Fig. 7 approach unity. In other words, in the limit, the excitation period equals the period of the structural mode. Note that the accuracy of the HB solution improves as the ratio $f\Delta t/\zeta$ increases.

Figure 8 shows the nondimensional excitation pulse width t_p/t_e given the nondimensional excitation period. The pulse widths for both stable and unstable limit cycles are indicated, but the excitation periods for the two states are approximately equal only when $f\Delta t/\zeta$ and $z_{cr}-z_0$ are both large (Fig. 7). The maxima of the curves in Fig. 8 correspond to the largest separation between the critical and quasi-steady deflections for which LCO is possible. Note that the pulse width at this limiting value approaches $t_e/4$ as ft_e (and, hence, $f\Delta t/\zeta$) increases. The pulse width for the stable limit-cycle state approaches $t_e/2$ when the critical and quasi-steady deflections are equal. It can also be concluded from Fig. 8 that, provided the value ft_e is fixed, the HB solution for the pulse width is in good agreement with the multifrequency solution.

Figure 9 shows AF_1 and AF_2 as a function of the ratio $f\Delta t/\zeta$. These values, when added to the quasi-steady deflection yield the maximum and minimum responses for the limit-cycle states (Figs. 2 and 3a). The HB solution underpredicts and overpredicts the AFs for the stable and unstable limit-cycle states, respectively. The multifrequency and HB solutions for stable limit cycles become linear (and independent of $z_{cr}-z_0$) as the ratio $f\Delta t/\zeta$ increases. It is easy to show, using the HB solution, that t_p/t_e tends to one-half and that the limits of AF_1 and AF_2 are given by

$$AF_1 = -\tfrac{1}{2} - f\Delta t/\zeta, \qquad AF_2 = -\tfrac{1}{2} + f\Delta t/\zeta \tag{22}$$

A single AF characterizes LCO induced by symmetric flow-state oscillations because the minimum and maximum responses are equal but of opposite sign (Fig. 1). Reference 6 shows that this AF converges to $AF = 2f\Delta t/\zeta$ as $f\Delta t/\zeta$ increases. The limits for symmetric and asymmetric flow-state oscillations, therefore, are related by

$$AF_s = 2AF_a + 1 \tag{23}$$

That is, the symmetric problem generates a response amplitude that is roughly twice that for the asymmetric problem. This conclusion is intuitively correct: In the symmetric problem, there are two force pulses ξ_p and four force lags ξ_l (Fig. 1). The symmetric problem, hence, has twice as many force lags as the asymmetric problem. Twice the amount of work is consequently conducted in each response cycle.

It can also be shown using the HB solution that the pulse width for the unstable limit cycle vanishes as $f\Delta t/\zeta$ increases and that AF_1 and AF_2 approach z_0-z_{cr} and $z_{cr}-z_0$, respectively. The maximum response for the unstable limit-cycle state, therefore, tends to z_{cr}. In other words, the response just reaches z_{cr}, which generates an infinitesimal force pulse. This conclusion is corroborated by the dashed curves in Fig. 8 and is illustrated in Fig. 4a.

Effects of Critical Deflection

Curves of the amplitude of the stable and unstable limit cycles, constructed using the multifrequency solution, are shown in Fig. 10 as a function of the control parameter $z_{cr}-z_0$. Initial responses that lie within the dark triangular region fail to balance the energy dissipation from structural damping and yield trajectories in the phase plane that spiral toward the stable fixed point z_0, designated by the x axis (see Figs. 3a and 4a). Initial responses that lie within the lighter region yield trajectories that approach the stable limit cycle, designated by the heavy solid lines (see Figs. 3b, 3c, 4b, and 4c). The two bifurcation points indicated in Fig. 10 are associated with unique $z_{cr}-z_0$ values as will be discussed.

The solution space shown in Fig. 10 is very similar to that for a mass riding on a driving belt that is operating at a constant velocity.[17] The friction force for this stick-slip system depends on the velocity of the mass relative to that of the driving belt. The relative velocity is a control parameter[17] analogous to $z_{cr}-z_0$ in the present problem.

Saddle-Node Bifurcation Point

As shown in Fig. 10, a limit cycle does not exist if the parameter $z_{cr}-z_0$ exceeds approximately $f\Delta t/2\zeta$. In this case, the work conducted during the force lags is insufficient to produce a steady-state response that exceeds the critical displacement z_{cr}. The response, thus, converges to the quasi-steady deflection z_0. Note that, at this

limiting value of the control parameter, the stable and unstable limit-cycle states are identical. That is, this point in the solution space represents a fold, or saddle-node bifurcation of cycles.[18]

Subcritical Hopf Bifurcation Point

The condition in which the critical deflection equals the quasi-steady deflection, that is, $z_{cr} \equiv z_0$, is also of special interest. In this case, the unstable limit cycle disappears. Small-amplitude oscillations near z_0 that used to vanish now grow until they reach the large-amplitude stable limit cycle. This behavior is characteristic of subcritical Hopf bifurcation (see Ref. 18).

As mentioned earlier, the oscillating flow separation force can be converted into aerodynamic stiffness and damping terms.[8,9] Equation (2) can, therefore, be rewritten as[8,9]

$$\ddot{z}(t) + 2\omega(\zeta + \dot{n})\dot{z}(t) + \omega^2(1+n)z(t) = 0 \tag{24}$$

where

$$n = -\xi_p/z, \qquad \dot{n} = -\omega\xi_l/2\dot{z} \tag{25}$$

Effective stiffness and damping are examined in detail in Refs. 8 and 9 for the semi-empirical model shown in Fig. 1. It is easy to verify using Figs. 2 and 6 that n and $\dot{n}$ are positive and negative, respectively, provided that the oscillating flow separation force is out of phase with the structural response. Effective frequency and damping of the limit-cycle state are, therefore, higher and lower, respectively, than the natural frequency and structural damping values of the mode.

It is also readily apparent that n and $\dot{n}$ are discontinuous within the response cycle. The HB solution, however, leads to constant values for these parameters because it implicitly linearizes the equation of motion.[8,9] If this smearing of the effects of the force pulses and lags is adopted, it is evident that Eq. (24) corresponds to free vibration of a linear system with effective frequency and damping values defined by[8,9]

$$\omega_e = \omega\sqrt{1+n}, \qquad \zeta_e = \zeta + \dot{n} \tag{26}$$

Indeed, at both the stable and unstable limit-cycle states, the effective damping value is precisely zero, which reflects that only undamped free vibration can emulate the steady-state forced response.[8,9]

The eigenvalues of the Jacobian matrix for Eq. (24), when evaluated at the fixed point $(z, \dot{z}) = (z_0, 0)$, are given by[9]

$$\lambda = -\zeta_e\omega \pm i\omega\sqrt{(\omega_e/\omega)^2 - \zeta_e^2} \tag{27}$$

When $z_0 < z(0) < z_{cr}$, the response does not induce the force ξ. Therefore, $n = \dot{n} = 0$, $\omega_e = \omega$, and $\zeta_e = \zeta$. The real part of the complex conjugate pair λ is consequently negative, which means that the fixed point is stable.[18] However, when $z(0) = z_0 = z_{cr}$, the force ξ is induced, and the aerodynamic damping term $\dot{n}$ is very large and negative.[9] The complex conjugate pair λ, therefore, "jumps" suddenly over the imaginary axis and into the positive real half of the complex plane.[17] This transition of positive-to-negative effective damping for the linearized system (and the attendant behavior of the eigenvalues of the Jacobian matrix) is emblematic of Hopf bifurcation (see Refs. 17 and 18). Discontinous bifurcations of this type are common in motion-dependent mechanical problems and are addressed comprehensively in Ref. 17.

Conclusions

Asymmetric flow-state oscillations coupled with the response of a single structural mode can be characterized as a weakly nonlinear system. The problem is amenable to analysis using a multifrequency trial function defined by the steady-state response of a linear oscillator subjected to a semi-empirical, analytic force. The multifrequency solution is in very good agreement with results from numerical solution of the equation of motion.

HB using a single term in the Fourier expansion of the idealized unsteady force is generally not as accurate as the multifrequency solution, but yields useful relationships for the limits of the solution space. The convergence of the first-order HB and multifrequency solutions also suggests that a first-order multiple scales[16] approximation could be used to study the evolution of the transient response to the limit-cycle state for cases in which $f\Delta t/\zeta \gg 2(z_{cr}-z_0)$. In other words, an analysis similar to that presented in Ref. 9 could be conducted for asymmetric flow-state oscillations. (Dotson[9] shows that if the product of the natural frequency and stuctural damping is low, the modal response generally will not reach the limit-cycle state unless the structure dwells in the transonic region.)

A stable fixed point, corresponding to quasi-steady deflection of the structural mode, is generally surrounded in the phase plane by an unstable and a stable limit cycle. The force–response coupling model used herein indicates that critical deflection values $z_{cr} = z_0$ and $z_{cr} = z_0 + f\Delta t/2\zeta$ correspond to a subcritical Hopf bifurcation point and a saddle-node bifurcation point, respectively. The location of the saddle-node bifurcation will differ when other models of the flow-state transition are used. It can be concluded that these phase-plane features may exist in aeroelastic phenomena due solely to the presence of a time lag during the change from one aerodynamic flow state to another.

Appendix: HB Solution

A solution of the nonlinear equation of motion based on HB[16] is provided for comparison with expressions from the multifrequency technique.

Series Expansion

It can be shown that the Fourier series expansion of the function ξ (Fig. 2) is given by

$$\xi(\tau) = -\frac{(t_p' - \Delta t)}{t_e} + \sum_{n=1,2,\ldots}^{\infty} a_n \cos(\omega_n\tau) \tag{A1}$$

where $\omega_n = 2n\pi/t_e$ and

$$a_n = (-1)^{n+1}\frac{2}{n\pi}\frac{\sin(\omega_n\Delta t/2)}{\omega_n\Delta t/2}\sin\left[\frac{\omega_n(t_p' - \Delta t)}{2}\right] \tag{A2}$$

Only the leading harmonic in the expansion is used herein; in other words, terms with $n \neq 1$ are ignored.

The admissible harmonic displacement is given by

$$z = z_m + b\cos[\omega_e(\tau + \Delta t/2)] \tag{A3}$$

in which the mean term z_m, the constant b, and the frequency ω_e will be defined by balancing coefficients in the nonlinear equation of motion. Note that, according to Eq. (A3), the response is approximated by a shifted cosine function oscillating about a constant value.

General Solution

Substituting Eqs. (A1), with $n = 1$, and (A3) into Eq. (2) yields

$$b\left[1 - (\omega_e/\omega)^2\right]\cos[\omega_e(\tau + \Delta t/2)] - b(2\zeta\omega_e/\omega)\sin[\omega_e(\tau + \Delta t/2)]$$
$$+ z_m = -(t_p' - \Delta t)/t_e + a_1\cos(\omega_e\tau) \tag{A4}$$

Equating the constant terms on the left- and right-hand sides of Eq. (A4) yields

$$z_m = -(t_p' - \Delta t)/t_e \tag{A5}$$

The sine and cosine functions on the left-hand side of Eq. (A4) are next expanded into terms involving $\cos(\omega_e\tau)$ and $\sin(\omega_e\tau)$. Equating the resulting coefficients of $\sin(\omega_e\tau)$ on the left- and right-hand sides of Eq. (A4) yields

$$(\omega_e/\omega - \omega/\omega_e)\tan(\omega_e\Delta t/2) = 2\zeta \tag{A6}$$

Similarly, the coefficients of $\cos(\omega_e\tau)$ yield

$$b = \frac{2}{\pi}\left(\frac{\omega^2}{\omega^2 - \omega_e^2}\right)\frac{\sin(\omega_e\Delta t)}{\omega_e\Delta t}\sin[\omega_e(t_p' - \Delta t)/2] \tag{A7}$$

Equation (A6) establishes the excitation period ($t_e = 2\pi/\omega_e$) but is independent of the pulse width t'_p. HB, therefore, predicts that the periods of the stable and unstable limit-cycle states, which have different pulse widths, are identical. Recall that this is not true for the multifrequency solution or for the numerical results (Fig. 7 and Table 1).

The requirement that the response equal the critical value at the time point t_a establishes the pulse width t'_p. Equation (A3), therefore, provides the relationship

$$z_{cr} = z_m + b\cos[\omega_e(t_a + \Delta t/2)] + z_0 \tag{A8}$$

Evaluating Eq. (A8) yields

$$z_{cr} - z_0 = -(t'_p - \Delta t)/t_e + \frac{1}{\pi}\left(\frac{\omega^2}{\omega_e^2 - \omega^2}\right)\frac{\sin(\omega_e \Delta t)}{\omega_e \Delta t}\sin[\omega_e(t'_p - \Delta t)] \tag{A9}$$

Equation (A3) indicates that the AFs (Fig. 2) are defined by

$$AF_1 = z_m + b, \qquad AF_2 = z_m - b \tag{A10}$$

such that

$$z_{min} = z_0 + AF_1, \qquad z_{max} = z_0 + AF_2 \tag{A11}$$

Simplifications for Negligible Force Ramp

As discussed in the text, the simplification $\omega\Delta t \approx 0$ is appropriate when the time lag is small relative to the period of the structural mode or when the force–response coupling is modeled as a pure step function that lags the critical response. In this case, Eq. (A6) yields the following explicit equation for the nondimensional excitation period:

$$f t_e = 1\Big/\sqrt{1 + 4\zeta/\omega\Delta t} \tag{A12}$$

Making use of this expression in the simplified form of Eq. (A7) yields

$$b = -(f\Delta t/\zeta)\sin(\pi t_p/t_e) \tag{A13}$$

Finally, the pulse width t_p is defined by the following simplified form of Eq. (A9):

$$z_{cr} - z_0 = -t_p/t_e + (f\Delta t/2\zeta)\sin(\omega_e t_p) \tag{A14}$$

Unlike the multifrequency technique [see Eq. (14)], HB does not yield an explicit expression for the nondimensional pulse width t_p/t_e.

The magnitude of the work conducted during the force lags depends on the form of the flow-state transition. The ratio $f\Delta t/\zeta$, therefore, should be scaled if Eqs. (A12–A14) are applied for transition models other than that shown in Fig. 2.

References

[1]Robertson, J. E., and Chevalier, H. L., "Characteristics of Steady-State Pressures on the Cylindrical Portion of Cone–Cylinder Bodies at Transonic Speeds," Arnold Engineering Development Center, Rept. AEDC TDR-63-104, Tullahoma, TN, Aug. 1963.

[2]Chevalier, H. L., and Robertson, J. E., "Pressure Fluctuations Resulting from an Alternating Flow Separation and Attachment at Transonic Speeds," Arnold Engineering Development Center, Rept. AEDC TDR-63-204, Tullahoma, TN, Nov. 1963.

[3]Cunningham, A. M., Jr., and Meijer, J. J., "Semi-Empirical Unsteady Aerodynamics for Modeling Aircraft Limit Cycle Oscillations and Other Non-Linear Aeroelastic Problems," *International Forum on Aeroelasticity and Structural Dynamics 1995*, Vol. 2 (A95-42613 11-39), Royal Aeronautical Society, London, 1995, pp. 74.1–74.14.

[4]Meijer, J. J., and Cunningham, A. M., Jr., "Outline and Applications of a Semi-Empirical Method for Predicting Transonic Limit Cycle Oscillation Characteristics of Fighter Aircraft," *International Forum on Aeroelasticity and Structural Dynamics 1995*, National Aerospace Lab., Rept. NLR-TP-95308-U, Amsterdam, 1995, pp. 75.1–75.19.

[5]Cunningham, A. M., Jr., "The Role of Non-Linear Aerodynamics in Fluid–Structure Interaction," AIAA Paper 98-2423, June 1998.

[6]Dotson, K. W., Baker, R. L., and Sako, B. H., "Launch Vehicle Self-Sustained Oscillation from Aeroelastic Coupling, Part 1: Theory," *Journal of Spacecraft and Rockets*, Vol. 35, No. 3, 1998, pp. 365–373.

[7]Dotson, K. W., Baker, R. L., and Bywater, R. J., "Launch Vehicle Self-Sustained Oscillation from Aeroelastic Coupling, Part 2: Analysis," *Journal of Spacecraft and Rockets*, Vol. 35, No. 3, 1998, pp. 374–379.

[8]Dotson, K. W., Baker, R. L., and Sako, B. H., "Launch Vehicle Buffeting with Aeroelastic Coupling Effects," *Journal of Fluids and Structures*, Vol. 14, No. 8, 2000, pp. 1145–1171.

[9]Dotson, K. W., "Transient Coupling of Launch Vehicle Bending Responses with Aerodynamic Flow State Variations," *Journal of Spacecraft and Rockets*, Vol. 38, No. 1, 2001, pp. 97–104.

[10]Oswald, J., David, F., and Ruffino, F., "Experimental and Numerical Simulation of an Oscillating Generic Launcher," *Premier Colloque Européen sur la Technologie des Lanceurs "Vibration des Lanceurs,"* ONERA, Rept. TP 2000-4, Toulouse, France, Dec. 1999.

[11]Bendiksen, O. O., "Transonic Flutter," AIAA Paper 2002-1488, April 2002.

[12]Wiercigroch, M., "Mathematical Models of Mechanical Systems with Discontinuities," *Applied Nonlinear Dynamics and Chaos of Mechanical Systems with Discontinuities*, edited by M. Wiercigroch and B. de Kraker, Series A, Nonlinear Science, Vol. 28, World Scientific, Singapore, 2000, pp. 17–38.

[13]Shaw, S. W., and Holmes, P. J., "A Periodically Forced Piecewise Linear Oscillator," *Journal of Sound and Vibration*, Vol. 90, No. 1, 1983, pp. 129–155.

[14]Natsiavas, S., "Dynamics of Piecewise Linear Oscillators," *Applied Nonlinear Dynamics and Chaos of Mechanical Systems with Discontinuities*, edited by M. Wiercigroch and B. de Kraker, Series A, Nonlinear Science, Vol. 28, World Scientific, Singapore, 2000, pp. 127–153.

[15]Dotson, K. W., Veletsos, A. S., and Ventura, C. E., "Dynamic Response of Simple Linear Systems to Periodic Forces," *Structural Research at Rice*, Dept. of Civil Engineering, No. 26, Rice Univ., Houston, TX, 1983.

[16]Nayfeh, A. H., and Mook, D. T., *Nonlinear Oscillations*, 1st ed., Wiley, New York, 1995, pp. 56–61.

[17]Leine, R. I., Van Campen, D. H., and Van De Vrande, B. L., "Bifurcations in Nonlinear Discontinuous Systems," *Nonlinear Dynamics*, Vol. 23, No. 2, 2000, pp. 105–164.

[18]Thompson, J. M. T., and Stewart, H. B., *Nonlinear Dynamics and Chaos*, 1st ed., Wiley, New York, 1986, pp. 111–121.

H. M. Atassi
Associate Editor